Received: 11 January 2023 | Revised: 21 April 2023 | Accepted: 18 May 2023

DOI: 10.1002/jnr.25220

RESEARCH ARTICLE

JOURNAL OF Neuroscience Research

A quantitative approach to study the adaptation of rhythmic eye movements and the resulting tonic eye deviation in larval zebrafish

Ting-Feng Lin[1,2] | Melody Ying-Yu Huang[1,2]

[1]Department of Neurology, University Hospital Zurich, University of Zurich, Zurich, Switzerland

[2]Neuroscience Center Zurich (ZNZ), University of Zurich and ETH Zurich, Zurich, Switzerland

Correspondence
Ting-Feng Lin, Department of Neurology, University Hospital Zurich, University of Zurich, Zurich, Switzerland.
Email: tingfenglin@uchicago.edu

Present address
Ting-Feng Lin, Department of Neurobiology, The University of Chicago, Chicago, Illinois, USA
Melody Ying-Yu Huang, Department of Health Sciences and Technology, Swiss Federal Institute of Technology (ETH) Zürich, Zürich, Switzerland
Melody Ying-Yu Huang, Department for BioMedical Research, University of Bern, Bern, Switzerland; and
Melody Ying-Yu Huang, Department of Anaesthesiology and Pain Medicine, Inselspital, Bern University Hospital, University of Bern, Bern, Switzerland

Funding information
Betty and David Koetser Foundation for Brain Research; Dr. Dabbous Foundation; EMDO Stiftung; Faculty of Medicine, UZH; Inselspital, Universitätsspital Bern

Abstract

To optimize performance during vital tasks, animals are capable of tuning rhythmic neural signals that drive repetitive behaviors, such as motor reflexes under constant sensory stimuli. In the oculomotor system, animals track the moving image during slow phases while repetitively resetting the eye position from the eccentricity during quick phases. During optokinetic response (OKR), larval zebrafish occasionally show a delayed quick phase; thus, the eyes remain tonically deviated from the center. In this study, we scrutinized OKR in larval zebrafish under a broad range of stimulus velocities to determine the parametric property of the quick-phase delay. A prolonged stimulation revealed that the slow-phase (SP) duration—the interval between two quick phases—was tuned increasingly over time toward a homeostatic range, regardless of stimulus velocity. Attributed to this rhythm control, larval zebrafish exhibited a tonic eye deviation following slow phases, which was especially pronounced when tracking a fast stimulus over an extended time period. In addition to the SP duration, the fixation duration between spontaneous saccades in darkness also revealed a similar adaptive property after the prolonged optokinetic stimulation. Our results provide a quantitative description of the adaptation of rhythmic eye movements in developing animals and pave the way for potential animal models for eye movement disorders.

KEYWORDS
adaptation, larval zebrafish, optokinetic response, quick phase, spontaneous saccade

1 | INTRODUCTION

To perform repetitive behavior, animals are capable of generating rhythmic commands within local circuits; however, animals are living in a dynamic environment, and therefore, the interval between rhythmic commands should be adjustable and adaptable according to the stimulus conditions (Dickinson, 2006; Pearson, 2000). For instance, when animals are exposed to a prolonged stimulus, they should be able to adapt the corresponding responses to save energy and seek the re-equilibrium. Thus, in response to the sustained

Edited by Junie Paula Warrington and Sokol Todi. Reviewed by Yuchin Albert Pan, Markus Tschopp, Aristides B. Arrenberg, and Vasileios Toulis.

stimuli, the brain should come up with a good decision of how to act regarding when, how often, and to which extent the behavior(s) should be executed. For example, the latency of saccadic eye movements is decided by modulatory factors from both the external environment and from inside the body, and that may also change over time.

In the current study, we investigated the rhythmic adaptation of saccadic eye movements under a prolonged stimulus in larval zebrafish. In their natural environment, zebrafish live in shallow, mostly clear water, which can be as steady as rice fields or the opposite like flowing hill streams (Spence et al., 2006), where they rely heavily on vision-driven motor behaviors such as optokinetic response (OKR) or optomotor response to adapt to the diverse environment. During these behaviors, zebrafish move their eyes or body according to the visual input to stabilize retinal images. OKR consists of slow phases that track the moving images and quick phases that reset the eye position (Figure 1). The two phases repetitively alternate when the stimulus continues.

During the OKR slow phase, eye velocity depends on stimulus velocity (Huang et al., 2006; Qian et al., 2005), and the slow-phase signal can further determine the latency of the quick phase (Kitama et al., 1992; Waddington & Harris, 2013, 2015). The mathematical relationship between stimulus velocities and the corresponding slow-phase (SP) duration has been examined in several studies (Waddington & Harris, 2013, 2015), which also reveals how the quick phase resets

Significance

Optokinetic response (OKR) is a reflexive eye tracking behavior of a large moving visual field, which is well conserved across most vertebrate taxa. During OKR, animals use quick phases to reset their eye position while tracking moving images. Intriguingly, young zebrafish larvae often display a tonic eye deviation at the eccentricity during the end of slow phases, instead of timely quick phases. In this study, we conducted a systematic assessment of the rhythmic saccadic eye movements in relation to optokinetic stimulation. Our findings not only provide a hitherto unavailable parametric reference critical for future experimental designs using the larval zebrafish oculomotor model but also offer new insights into saccade deficiencies in an underdeveloped brain such as congenital ocular motor apraxia in young children.

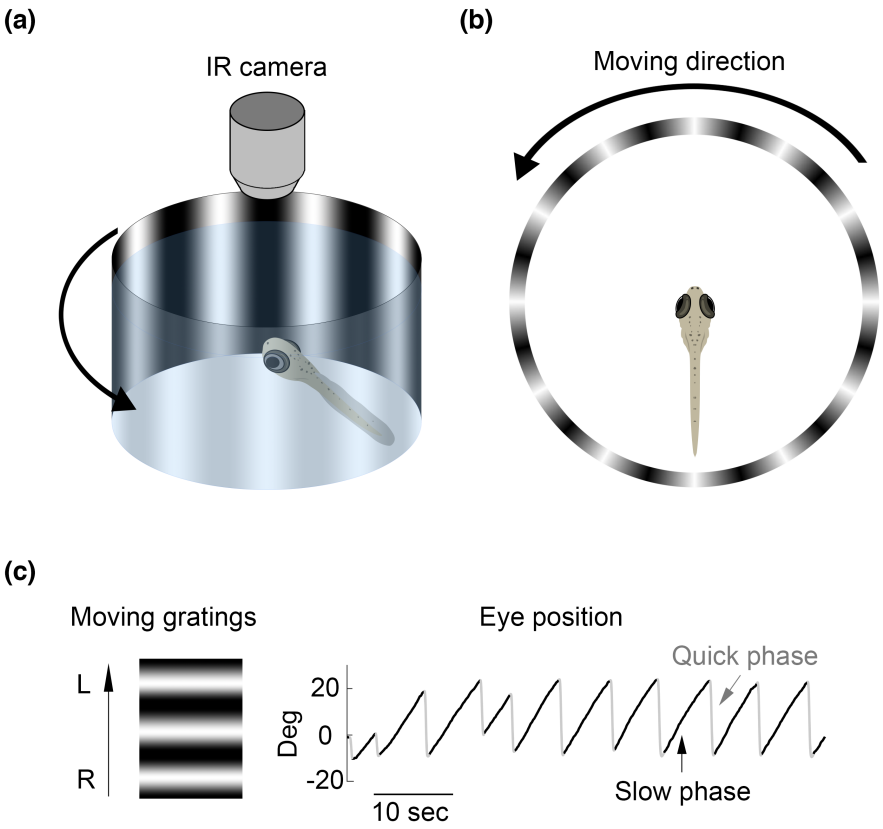

FIGURE 1 Experimental setup and the recorded optokinetic eye movements. (a) Schematic drawing that depicts the experimental setup to record OKR in larval zebrafish. A larval zebrafish was embedded in the center of an optokinetic cylinder projected with a black and white grating pattern with a spatial frequency of 0.053 cycles/°. Horizontal eye movements were recorded using an IR camera on top. (b) Top view of (a) through the IR camera. (c) The demonstrated eye position trace showing the slow phase and quick phase of OKR. Movements to the left (counterclockwise) are represented by positive values, while movements to the right (clockwise) are represented by negative values. IR, infrared; OKR, optokinetic response; s, second.

the eye position within an appropriate time range. Nonetheless, Baker and colleagues demonstrated an occasional delayed quick phase in larval zebrafish (Beck et al., 2004). In our previous study, we have shown that both SP velocity and SP duration adapt to a prolonged stimulus; however, across stimulus time span, the adapted magnitudes of these two parameters are not linearly correlated (see Figure S2 from Lin et al., 2019), suggesting that SP velocity is not an ideal predictor for SP duration. In addition to SP velocity, SP duration or its reciprocal (i.e., frequency) is often used to indicate the efficiency of optokinetic eye tracking (Page-McCaw et al., 2004; Wu et al., 2020). However, this nonlinearity may lead to discrepancy and imprecision while choosing different SP parameters to assess optokinetic behavior. Although studies on the zebrafish optokinetic system are increasing rapidly, the basic characteristic of such behavior is not well described. Furthermore, this nonlinearity also brings into question how brains decide the timing of the quick phase based on stimulus velocity over a prolonged stimulation period.

In the current study, we recorded the SP duration under different stimuli for 10 min. In parallel with the adaptation of SP velocity, the SP duration increased over time until reaching a plateau value of around 10 s, regardless of the SP velocity or the stimulus velocity, leading to a tonic eye deviation. Furthermore, the adapted SP duration closely matched the pre-stimulus fixation duration between two spontaneous saccades in darkness. Although spontaneous saccade can be initiated by an internal generator, our data revealed that the prolonged optokinetic stimulus can also modulate the spontaneous saccade frequency, indicating a concurrent adaptation of both saccadic eye movements to the same external stimulus.

2 | MATERIALS AND METHODS

2.1 | Fish breeding and upkeep

In accordance with the Federal Veterinary Office of Switzerland (FVO) guidelines—TSchV art. 112, no ethical approval is required for studies on larvae under the age of 120 h/5 days post fertilization prior to the independent feeding. AB and TU wild-type zebrafish lines were purchased from the zebrafish breeding facility at European Zebrafish Resource Center (EZRC) and maintained under a cycle of 14 h light/10 h darkness in 28°C E3 medium (5 mM NaCl, 0.17 mM KCl, 0.33 mM CaCl2, and 0.33 mM MgSO4) as previously described (Haffter et al., 1996; Mullins et al., 1994). For the experiments, individual zebrafish larvae were randomly selected from clutches 5 days post fertilization, prior to the independent feeding.

2.2 | Visual stimulation and recording

All experiments were performed between 8:00 AM and 7:00 PM following the environmental light/darkness cycles. During the recording, larval zebrafish were restrained in low-melting agarose (Sigma Type VII-A) without constraining the eyes, as described previously (Lin et al., 2019). OKR was evoked by the moving images projected on a transparent screen by four digital light projectors (Samsung SP-H03 Pico Projector). The moving images consisted of a black and white vertical sinusoid grating pattern with a spatial frequency of 0.053 cycles/°. The black and white contrast is 100% and the maximum illumination is 1524 lux. The larvae were placed on a transparent glass plate submerged in water and illuminated from the bottom with infrared (IR)-emitting diodes (λpeak = 875 ± 15 nm, OIS-150880, OSA Opto Light GmbH, Germany). The eye positions were captured at a sampling rate of 40 frames/s using an IR-sensitive charge-coupled device (CCD) camera. The area of the eyes as the region of interest was detected by brightness/contrast and adjusted manually. The stimulus was controlled and the eye position images were captured and processed by a custom-made program written in LabVIEW (National Instruments, Austin, Texas, USA) (Chen et al., 2014).

Throughout this study, the spontaneous eye movements were recorded in darkness for 5 min before the stimulation. To test the dependency of eye movements on stimulus velocity, the larvae were exposed to 10 min of unidirectional optokinetic stimulus to the left (counterclockwise) different velocities (10, 20, 40, 60, and 80 °/s). To test the SP durations under prolonged stimulation, larvae were exposed to 30 min of unidirectional optokinetic stimulus at 10 °/s. To test the effect of SP duration adaptation on fixation duration in darkness, the larvae were exposed twice to 20 min of directionally alternating optokinetic stimulus, with 5 min of darkness in between. The stimulus velocity was 10 °/s, and the direction alternated every 15 s. Fixation duration was tested for 5 and 10 min before and after two episodes of stimulations, respectively.

2.3 | Data analysis

Throughout this paper, the positive value corresponds to the left (counterclockwise) direction. The collected data were analyzed on MATLAB (MathWorks, Natick, MA, USA). Eye position traces were smoothened by a Gaussian filter with a cutoff frequency of 5.5 Hz. The eye velocity traces were estimated as the derivative of eye position traces. Saccadic eye movements were identified with a velocity threshold of 20 °/s and a dislocation threshold of 1°, followed by manual adjustments as previously described (Lin et al., 2019). We estimated the SP/fixation duration or SP amplitude by quantifying the time span or eye dislocation between the end of the previous and the beginning of the next saccadic eye movements. To estimate the SP velocity of real eye tracking and exclude the eye drifting when eyes lodged eccentrically, we defined the SP velocity as the median velocity during the first second of each slow phase. If the slow phase was shorter than 1 s, then SP velocity was the median velocity across the whole slow phase. A comparison between an eye position trace and the estimated SP velocity slope (Figure 4c) confirms that the method used in this paper captures the actual eye tracking velocity very well.

To estimate the SP time constants (Figure 4a), we fitted the eye position of each individual slow phase with a first-order exponential decay function:

$$f(t) = -G \bullet e^{-\frac{t-ti}{\tau}} + \text{ecc} \quad (1)$$

where $f(t)$ represents the eye position function of time (t), G is the maximum range of eye movement in degree, ti denotes the initiation time of each slow phase, τ represents the time constant of the eye position change, and ecc refers to the most eccentric position that the eye can reach. The absolute value of the most eccentric position during the recording is denoted as ω. G is constrained by two ω, while ecc is constrained to be within $\pm(\omega+5)$. Phase-I duration was estimated as the quotient of SP amplitude divided by SP velocity (Figure 4b). To estimate phase-II duration, we subtracted the estimated phase-I duration from the entire SP duration.

To align the time variables across different recordings and create a standardized 40-Hz dataset, gaps in the estimates (i.e., SP durations, SP velocities, SP amplitudes, SP time constants, phase-I durations, and phase-II durations) between two slow phases were filled using linear interpolation, and the two ends of data were extrapolated as the nearest sample value. The differences between different time points of the same fish were tested using the Wilcoxon signed rank test. The differences among stimulus conditions were tested using the Kruskal–Wallis test, followed by the post hoc pairwise comparison tests using Dunn & Sidák's correction. Across the entire article, asterisks denote significant difference levels ($^{*}p<.05$; $^{**}p<.01$; $^{***}p<.001$; Wilcoxon signed rank test). The detailed values are provided in the supplementary tables if p is equal to or larger than 0.001.

To estimate the time constant of SP duration adaptation (Figure 7a and Figure S8a), we fitted SP duration under a 30-min stimulus of 10°/s with a first-order exponential decay function:

$$f(t) = G \bullet e^{-\frac{t-ti}{\tau}} + \text{offset} \quad (2)$$

where $f(t)$ represents SP duration function of time (t), G is the gain of adaptation, ti is the initiation of optokinetic simulation, τ is the time constant of adaptation, and "offset" is the saturated value of the adapted SP duration.

3 | RESULTS

3.1 | SP duration increased with optokinetic stimulation

To record OKR in larval zebrafish, we fixed the fish in low-melting agarose without restraining the eyes. We provided optokinetic stimulus by projecting a counterclockwise-moving sinusoidal grating onto a cylinder screen surrounding the fish (Figure 1a,b). During OKR, the quick phase resets eye position from a corner to a point closer to center, allowing space for the next slow phase (Figure 1c). However, under prolonged optokinetic stimulation, we often observed a delayed quick phase following eye tracking, in which the eyes remained tonically deviated at the most eccentric position. To better describe this behavior, we separated the slow phase into two episodes: phase I (actual eye tracking) and phase II (duration at eccentric position) (Figure 2a). Even though phase II is common and robust in larval zebrafish, only a few reports have mentioned it briefly without a quantitative analysis in detail (Beck et al., 2004; Ma et al., 2020).

To scrutinize this delayed quick phase under different stimulus velocities, larval zebrafish were exposed to 10 min of optokinetic stimulation at velocities of 10, 20, 40, 60, or 80°/s (Figure 2b–l). Within 1 min of stimulation, we observed a deceleration of the slow phase when the eyes approached the eccentric position. This behavioral effect occurred earlier with faster stimuli (40, 60, and 80°/s; Figure 2g,i,k). At the end of the 10-min OKR, faster stimuli produced a significant phase II (Figure 2h,j,l) compared with slower stimuli. However, it is not clear whether a slower stimulus (e.g., 10°/s) would eventually produce a noticeable phase II if the stimulus lasted longer.

To show the delayed quick phase quantitatively, we plot SP duration over time (Figure 3a). This reveals an early period of rapid increase within the initial 15–30 s (Figure 3b), followed by a prolonged later period with slow increase. The increase of SP duration over 10 min of OKR was statistically significant in all groups (Figure 3c). At the beginning of OKR, SP duration depended on stimulus velocity (Table S1, Figure 3c), with faster stimuli resulting in shorter SP durations. Contrarily, after 10 min of stimulation, faster stimuli led to a more robust increase in SP duration than slower stimuli, resulting in comparable SP durations at the end of the 10-min OKR under different stimulus velocities (Table S2 and Figure 3c). The early steady state, which was observed at around 30 s, exhibited similar trends to those observed at the end of the 10-min recording (data not shown). Since the focus of this research was on tonic eye deviation, we will only present comparisons between the beginning and end of recording in the following sections. The data shown in Figure 3a–c were collected from the right eye, and the data from the left eye are shown in Figure S1a–c.

Furthermore, we also demonstrate SP velocity and SP amplitude, which are factors used to determine SP duration. In this study, SP velocity specifically indicates the eye-tracking velocity during phase I (see Methods). During 40–80°/s stimuli, the SP velocities reached a peak within the first 5 s (Figure 3d,e). These peaks were followed by a rapid decay over 15 s and then a continuing slow decay. By contrast, the SP velocities under 10–20°/s of stimuli did not exhibit that transient high velocity at the beginning of OKR, and only showed the slow decay over a timescale of min. We separately quantified the peak SP velocity in the initial period and the following steady SP velocities (Figure 3f). Overall, SP velocity showed a dependency on the stimulus velocity under 40°/s and saturated for stimulus velocities over 40°/s. The data shown in Figure 3d–f were collected from the right eye, and the corresponding left eye data are shown in Figure S1d–f. The differences in SP velocities under stimulus conditions were significant

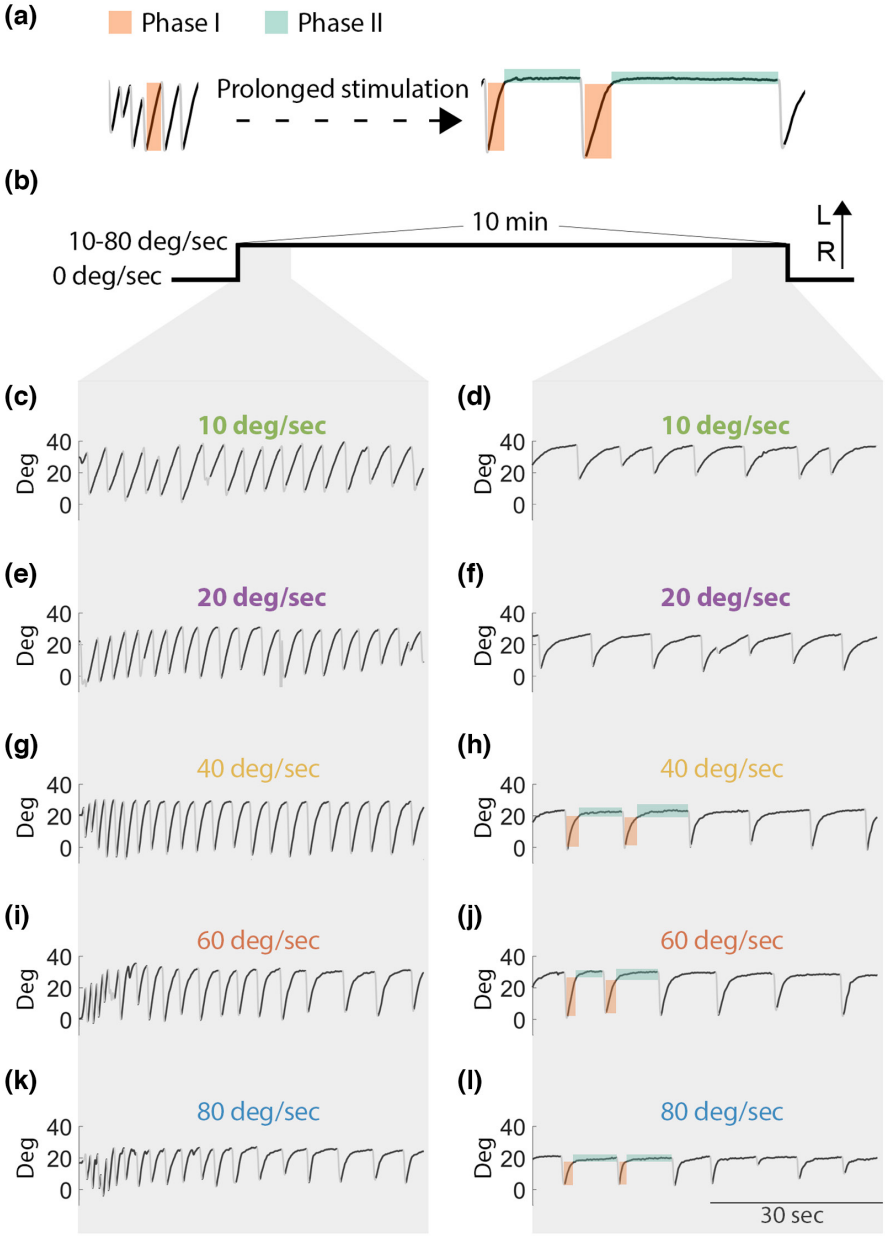

FIGURE 2 Prolonged optokinetic stimulation leads to an eye staying at the eccentric position following the image tracking without a timely position reset. (a) A demonstrated eye position trace showing the designated phase-I and phase-II slow phases during OKR. (b) A visual stimulation protocol of OKR with the stimulus velocities from 10 to 80°/s and (c–l) the corresponding eye position traces during the first and the last 1 min of the OKR stimulation. Phase I, highlighted by an orange-shaded area, is defined as the actual eye tracking. Phase II, highlighted by a green-shaded area, is defined as tonic eye deviation at the eccentric position of the eye orbit. Deg, degree; min, minute; OKR, optokinetic response; s, second.

(Tables S3 and S4). Note that in the current study, all stimulus velocities employed ultimately resulted in a SP gain of approximately 0.5 or lower value (Figure S2). In general, our data showed OKR trends similar to those of the previous studies (Huang et al., 2006; Qian et al., 2005), and the difference in values was expected due to various technical settings such as body restraint methods during the eye recordings.

In contrast to SP velocity, SP amplitude was rather stable throughout the recordings (Figure 3g). SP amplitudes increased within the first 5 s (Figure 3h), and then either remained at the same level or slowly decreased over time (Figure 3g). Figure 3i shows a comparison of average SP amplitudes between the first 5 s (early) and the last 5 s (late). Even though the SP amplitude value increased during the first 5 s until reaching a steady state (Figure 3h), only a few groups revealed a significant difference between the early and late periods (Figure 3i and Table S5). The data shown in Figure 3g–i were collected from the right eye, and the corresponding left eye data are shown in Figure S1g–i. Furthermore, SP amplitudes under various stimulus velocities were not significantly different (Tables S6 and S7).

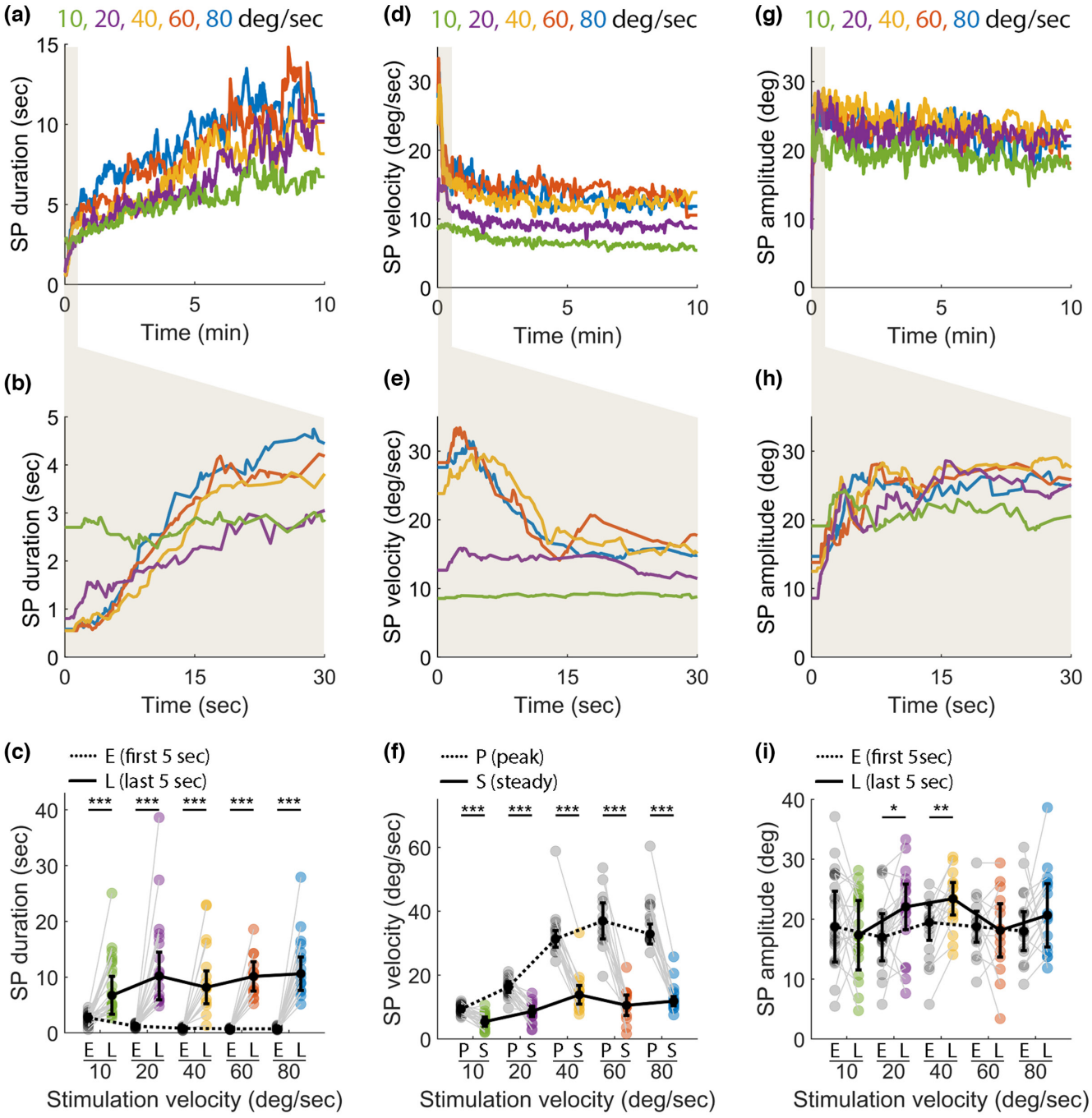

FIGURE 3 Ten minutes of stimulation leads to OKR adaptation. Right eye (a–c) SP duration, (d–f) SP velocity, and (g–i) SP amplitude under different stimulus velocities. Median of (a) SP durations, (d) SP velocities, and (g) SP amplitudes among fish during the 10-min recording under 10, 20, 40, 60, and 80-°/s stimuli ($n = 23$, 19, 16, 15, and 17, respectively). (b), (e), and (h) show the magnifications of (a), (d), and (g), respectively, to demonstrate the initial 30 s of recordings. (c), (f), and (i) plot the statistical results of SP durations, SP velocities, and SP amplitudes, respectively. P stands for peak SP velocities during the beginning of recordings. Average values during the first 5 s (early, E) and the last 5 s (late, L, or steady state, S) were calculated. Gray and colored circles indicate the values of individual fish. Black circles ± error bars indicate the median ± median absolute deviation of populations. The population medians are linked by dotted lines or solid lines across stimulus conditions. Asterisks denote the significant difference levels (*$p < .05$; **$p < .01$; ***$p < .001$; Wilcoxon signed rank test). Deg, degree; min, minute; OKR, optokinetic response; s, second; SP, slow phase.

3.2 | Extended duration of SP is not solely attributed to the SP velocity slowdown

Following the conventional method to determine the timescale of curved eye position trajectory (Miri et al., 2022), we estimated the time constant by fitting the eye position of each individual slow phase with an exponential fit (Figure 4a). Across all stimulus conditions in the 10-min OKR tasks, the time constant generally increased (Figure 4d–f and Table S8). Time constants were shorter when stimulus velocity was higher (Figure 4f, Figure S3c and Tables S9 and

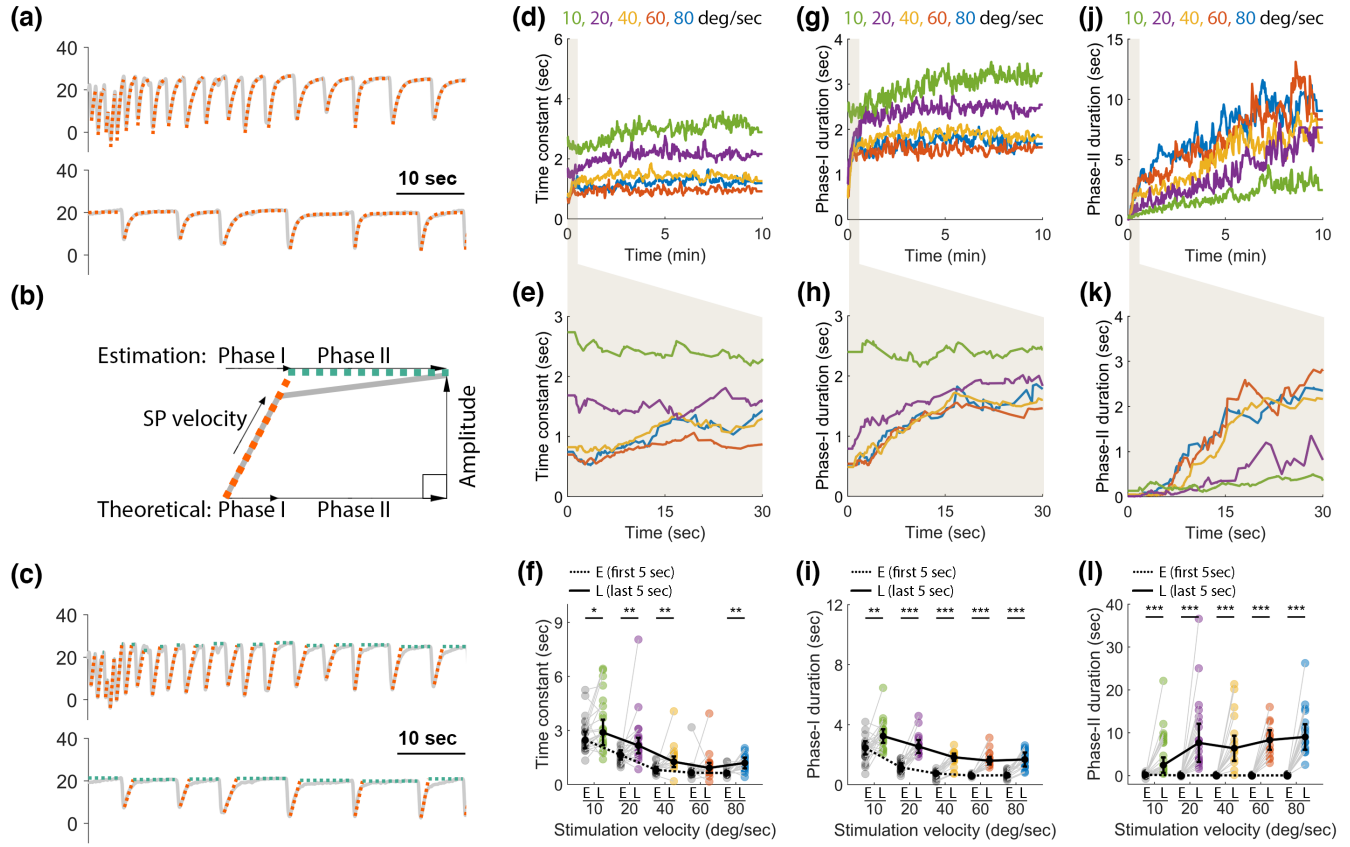

FIGURE 4 SP time constants, phase-I and phase-II durations extend over 10 min of optokinetic stimulation. (a) Representative eye position traces (gray lines) overlapped with first-order exponential fits (dotted red lines). (b) A schematic eye position trace demonstrating the strategy for estimating phase-I and phase-II durations. Phase-I duration is estimated by dividing SP amplitude over the SP velocity of the actual eye tracking, which is shown as the slope of the dotted red line. Phase-II duration (dotted green line) is estimated by subtracting phase-I duration from SP duration. (c) Representative eye position traces overlapped with the estimated phase-I (dotted red lines) and phase-II (dotted green lines) eye position. Right eye (d–f) SP time constant, (g–i) phase-I duration, and (j–l) phase-II duration under different stimulus velocities. The medians of (d) SP time constants, (g) phase-I durations, and (j) phase-II durations among fish during the 10-min recording under 10, 20, 40, 60, and 80-°/s stimuli ($n = 23$, 19, 16, 15, and 17, respectively). (e), (h), and (k) show the magnifications of (d), (g), and (j), respectively, to demonstrate the initial 30 s of recordings. (f), (i), and (l) plot the statistical results of SP time constants, phase-I and phase-II durations, respectively, during the first 5-s (early, E) and the last 5-s (late, L). Gray and colored circles indicate values of individual fish. Black circles ± error bars indicate the median ± median absolute deviation of populations. The population medians are linked by dotted line or solid line across stimulus conditions. Asterisks denote significant difference levels (*$p < .05$; **$p < .01$; ***$p < .001$; Wilcoxon signed rank test). The p-values comparing the early and late SP time constants are shown in Table S8. Additionally, the p-value of phase-I durations under 10 °/s is 0.002. Deg, degree; min, minute; s, second; SP, slow phase.

S10), which was consistent with the early SP duration but opposite to the late SP duration (Figure 3c). While the time constant provided information on the timescale of eye position change, it was insufficient to fully explain SP duration when the tonic eye deviation was apparent. To better scrutinize how phase I and phase II contribute to the entire SP duration, we used a quantitative approach to estimate the duration of each phase. Considering phase I represents the actual eye tracking and contributes to almost the entire SP amplitude, the quotient of SP amplitude divided by SP velocity can be used to approximate the time span of phase I (Figure 4b). Phase II duration was the estimated phase I duration subtracted from the entire SP duration. In Figure 4c, the slope of the estimated SP velocity overlapping the empirical eye position trace shows their proximity. The estimated phase-I and phase-II depicted on top of the eye position trace reveals that the method used in this study gives a fairly accurate estimate of the two phases.

In general, phase-I duration increased during the first 30 s and then was saturated–except during the 10 °/s stimulus (Figure 4g,h)–and the differences were confirmed by statistical tests (Figure 4i). We also observed that phase-I duration was dependent on stimulus velocity at both the beginning and end of recordings. Specifically, higher stimulus velocities led to shorter phase-I durations, and the differences among the conditions were significant (Tables S11 and S12). In rough terms, the trends and values of phase-I duration were similar to those of SP time constant, as both estimate the timescale of eye position changes. By plotting phase-I durations over SP time constants, we showed that there was a significant correlation between these two parameters (Figure S4a,b,e,f). Contrarily, as the

fish eyes did not show the tonic deviation in the beginning of OKR (Figure 2), the estimated phase-II durations were all around zero in the first 5 s, and then increased over time (Figure 4j–l). The faster stimulus led to a longer duration of phase II when recordings ended. As such, total SP duration is adjusted to a unifying range across stimulus conditions by a compensatory relationship between Phase I and Phase II durations (Figure 3c and Table S2). Contrary to phase-I duration, it is not surprising that both phase-II and SP durations showed lower correlations with SP time constant across all groups (Figure S4). The data discussed and shown in Figure 4d–l were collected from the right eye. The corresponding left eye data are shown in Figure S3.

The observation of Phase II, in which the eyes remained fixed at the eccentric position without triggering a quick phase, supports the hypothesis that the quick phase is scheduled by an oscillator, rather than being triggered based on an eye position threshold. To further examine this hypothesis, we analyzed the beating field to determine if quick phases were consistently initiated at a specific eye position. The beating field is depicted as the area from the beginning to the end of quick phases (Figure S5). Indeed, the beating field drifted throughout the OKR period, and the position where the quick phase was initiated varied. Specifically, in the beginning of the OKR, the left eye showed a beating field shift toward the stimulus direction (leftward), as previously reported (Chen et al., 2014), and the shift was brisker and more rapid under faster stimuli (Figure S5g–j). After the early leftward drift, the beating field shifted back slowly (Figure S5c–e). In comparison, the right eye only showed a similar shift when the stimulus was slow (10°/s; Figure S5a). When stimuli were equal to or faster than 20°/s, the beating field of the right eye initially expanded in both directions and then narrowed (Figure S5b–j).

3.3 | Spontaneous saccade frequency also adapts after a prolonged optokinetic stimulus

Although spontaneous saccade in darkness can be driven by an internal clock without sensory cues (Ramirez & Aksay, 2021), recent research suggests that the latency of these saccades may still be influenced by visual input (Kitama et al., 1992, 1995; Wolf et al., 2017). Thus, we tested if the fixation duration of spontaneous saccades in darkness was also modulated by the prolonged optokinetic stimuli as seen in the OKR quick phases. Similar to the SP duration estimation, we computed the fixation duration—defined as the period from the end of the previous saccade to the beginning of the next saccade—in darkness and compared the values before and after the prolonged optokinetic stimulation. Earlier we have shown that unidirectional optokinetic stimulation leads not only to an increase in the duration of SP but also to a post-stimulus optokinetic afternystagmus (Lin et al., 2019; Pérez-Schuster et al., 2016; Wu et al., 2020); thus, in the current study to avoid catching the optokinetic afternystagmus instead of post-stimulus spontaneous saccades, we trained larval zebrafish with direction-alternating optokinetic stimulation (Figure 5). After two episodes of 20-min optokinetic stimulation with a 5-min break in between (Figure 5a), the SP duration adapted and increased significantly (Figure 5b–d). In comparison to the pre-stimulus fixation durations, we observed a significantly longer fixation duration after the stimulation (Figure 5b,c,e). The data shown in Figure 5d,e were collected from the right eye, and the corresponding left eye data are shown in Figure S6.

Our findings revealed that the prolonged optokinetic stimulation not only affects the SP duration but as well the fixation duration in darkness, likely implicating interconnected circuits underlying spontaneous saccade and quick phase initiations. Nevertheless, further evidence on the cellular level will be still needed in the future.

3.4 | The adapted optokinetic SP duration is quantitatively close to the spontaneous fixation duration in darkness

According to our data, SP durations under all stimulus conditions were tuned to similar values through the OKR adaptation process (Figure 3c and Table S2). This raises a question whether there is a homeostatic control that adjusts saccadic frequencies to a preferred range regardless of visual conditions. Furthermore, since spontaneous saccades and quick phases might be initiated by shared or overlapping circuits, we wonder if spontaneous saccade frequency is preset within the same range. We compared SP durations in different time periods with the pre-stimulus fixation durations. Figure 6 depicts SP duration in the first 5 s and the last 5 s during OKR stimulation normalized by the pre-stimulus fixation duration. In the first 5 s, values of SP duration are smaller than the pre-stimulus fixation durations (Figure 6b and Table S14). Interestingly, in the last 5 s, there is no statistical difference between the adapted SP duration and the pre-stimulus fixation duration (Figure 6c and Table S14). The data shown in Figure 6 were collected from the right eye, and the corresponding left eye data are shown in Figure S6.

Since the SP duration continued to increase at the end of the 10-min recordings, especially under a slow stimulus velocity of 10°/s (Figure 3a), we further prolonged the OKR stimulus for 30 min. We sought to see if the SP duration stopped increasing at around the same value of the pre-stimulus fixation duration. Indeed, we observed that the extended SP duration reached a plateau within the first 20 min of OKR under the stimulus velocity of 10°/s (Figure 7a). We fitted the increasing curves with first-order exponential function. The estimated time constants with 95% confidence intervals are 373.5 ± 3.6 s for the right eye and 327.3 ± 3.2 s for the left eye. Similar to the previous results (Figure 6c), there is no significant difference between the SP duration at the end of a 30-min OKR and the pre-stimulus fixation duration (Figure 7b). The data shown in Figure 7 were collected from the right eye, and the corresponding left eye data are shown in Figure S8. These results reveal that, regardless of the various initial values under different stimulus velocities, SP duration is adjusted over time until it reaches a unifying value (Table S2) that is around the pre-stimulus fixation duration,

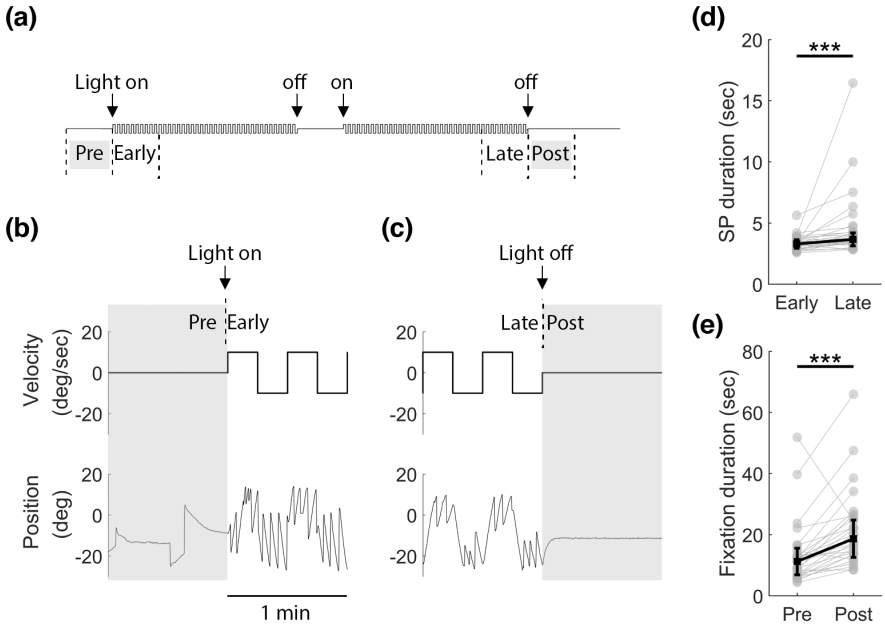

FIGURE 5 The extended fixation duration after SP-duration adaptation. (a) A visual stimulation protocol showing twice 20-min optokinetic stimulations interweaving with 5-, 5-, and 10-min darkness before, between, and after stimulation phases. The stimulus velocity is 10°/s, and the direction alternates every 15 s. (b) and (c) The demonstrated eye position traces showing the beginning and end of OKR under directionally alternating stimulation. On top of the eye position traces is the stimulus velocity. (d) The comparison of the SP durations between the first and last 5 min of the stimulation. (e) The comparison of fixation durations in darkness before and after the stimulation. Gray circles indicate average SP or fixation durations within each 5-min window of individual fish. Black circles ± error bars indicate median ± median absolute deviation of the population ($n = 29$). Asterisks denote the significant difference (***Wilcoxon signed rank test, $p < .001$). Data are collected from the right eye. Deg, degree; min, minute; OKR, optokinetic response; s, second; SP, slow phase.

likely implicating an underlying homeostatic control of the saccadic frequencies.

4 | DISCUSSION

4.1 | Optokinetic quick-phase delay should be treated carefully with slow-phase analysis

OKR is an important and conserved ocular motor behavior exhibited by various animal species (Huang & Neuhauss, 2008) and has been extensively studied in the past. Recently, an increasing number of OKR-related studies have been conducted in larval zebrafish. There are several advantages of using zebrafish as a model for oculomotor research. While recording larval OKR, however, we encountered a fundamental issue which hinders data analysis and interpretation. Specifically, after a prolonged stimulation (>1 min), the animal started to show tonic deviation of the eyes at an eccentric position after the slow phase, and eye tracking did not immediately lead to an eye position reset by a quick phase. As a result, the animal did not start the next slow phase in a timely manner.

This quick-phase delay may lead to ambiguous definition of the actual slow phase. Precisely, when computing the velocity gain of the eye tracking, which is a commonly used indicator of OKR efficacy, only the phase I should be considered as the true tracking period (Figure 2a). Besides velocity gain, calculating the difference between quick-phase frequencies in two directions (i.e., optokinetic response index) is an alternative indicator of OKR efficacy (Page-McCaw et al., 2004; Wu et al., 2020). However, since the adapted quick-phase frequency and adapted SP velocity across stimulus time span are not linearly correlated with each other, analysis of quick-phase frequency for prolonged optokinetic stimulation, especially under a faster stimulus, should be interpreted with care and adjusted based on individual studies.

4.2 | The adapted quick phase is initiated by a distinct mechanism than an eye position threshold

The delayed quick phase may shed light on the brain's algorithm of saccade initiation. Waddington and Harris described two models to explain the stochastic nature of the SP duration (Waddington & Harris, 2013): In the first model, the quick phase is initiated by an oscillator which relies on the accumulated decision signal to reach the threshold and generates periodic signals, and the intervals can be predicted by different probability density functions (Anastasio, 1996; Noorani & Carpenter, 2016; Trillenberg et al., 2002; Waddington & Harris, 2013). The second model proposes that a quick phase is triggered when eyes reach a position threshold during the slow phase. In that case, the SP duration would be decided by the ratio of the variable SP amplitude to the variable SP velocity. In our recording, phase II represents a distinct period when eyes are temporarily lodged eccentrically (i.e., the tonic

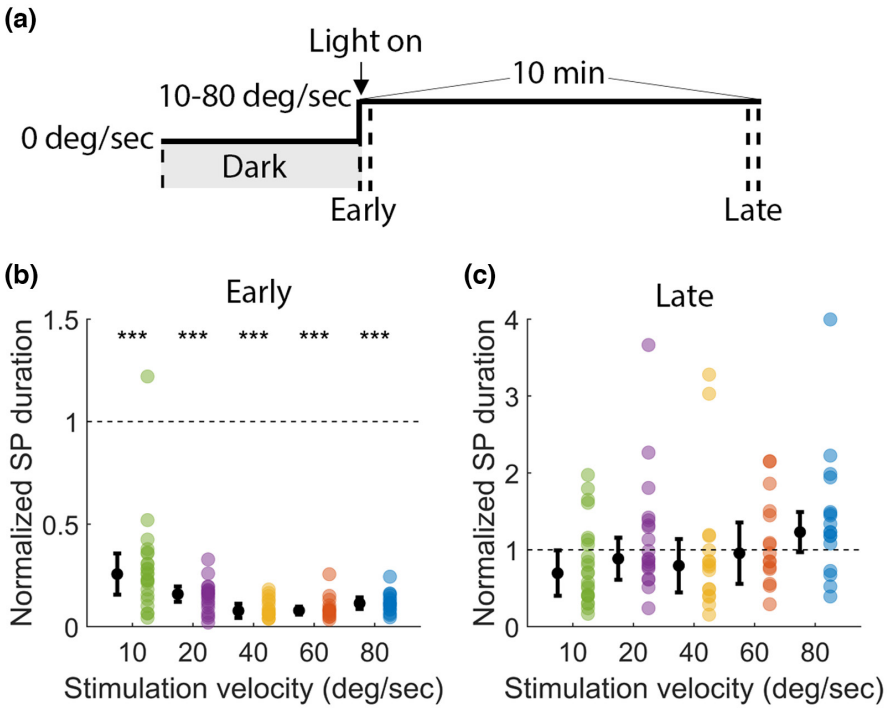

FIGURE 6 A comparison between the fixation duration in darkness and SP duration in different time periods. (a) A visual stimulation protocol showing 5-min darkness followed by 10 min of optokinetic stimulation with the stimulus velocities at 10, 20, 40, 60, and 80 °/s ($n = 23$, 19, 16, 15, and 17, respectively). (b) and (c) SP durations in the first 5 s (early) and the last 5 s (late) of OKR, respectively, normalized by the pre-stimulus fixation duration (dark). Colored circles indicate the normalized SP duration of individual fish. Black circles ± error bars indicate median ± median absolute deviation of populations. Asterisks denote significantly different than 1 (***Wilcoxon signed rank test, $p < .001$). Data are collected from the right eye. Deg, degree; min, minute; OKR, optokinetic response; s, second; SP, slow phase.

eye deviation), causing a nonlinear trajectory of the slow phase under a constant stimulus velocity (Figure 2a). This tonic deviation of the eyes suggests that quick-phase initiation does not (only) rely on the eye position, and therefore implies at least an additional distinct mechanism (i.e., oscillator) than the eye position threshold proposed in the second model. In addition to the models discussed above, there are also models used to explain rhythm generation in other behavioral studies. To describe the optomotor response in larval zebrafish, a stochastic model independent of input history was proposed by Portugues and colleagues (2015). In this model, command frequency of a stochastic rhythm generator can be regulated by sensory input instantaneously. A similar rhythm generator can be found at different levels of neural circuits. For example, Purkinje cells generate simple spikes spontaneously (Raman & Bean, 1999), but the firing rate can be regulated by synaptic inputs instantaneously (Otis, 2016).

Prior to saccadic eye movements, burst-driving neurons (BDNs) maintain a tonic firing rate and start to rise no earlier than 100–150 ms before spontaneous saccades (Kitama et al., 1992, 1995). This tonic firing does not appear to indicate a continuous accumulation of decision signals. However, with broad recording throughout the zebrafish hindbrain, a group of cells showed a ramping activity 1–13 s before the spontaneous saccades. In the same study, the ramping activity can be used for predicting fixation durations with a ramp-to-threshold model, which supports the idea of a temporal integration of the decision signal (Ramirez & Aksay, 2021). However, it is not known whether the ramping activity performs a similar function during the quick phase. In general, it remains debatable if the quick-phase initiation is the result of the temporal integration or an instantaneous process.

4.3 | Spontaneous saccades and quick phases show similarity in the temporal properties

Neuroanatomically, it is generally believed that OKR shares the same neural substrates, or follows the same sensorimotor controls, of the vestibular ocular reflex to generate a quick phase. Specifically, burst neurons process the slow-phase signals from vestibular nucleus neurons through BDNs to terminate the slow phase (Nakao et al., 1982) and initiate the quick phase (Fukushima et al., 1991; Kitama et al., 1992; Ohki et al., 1988). In zebrafish research, several studies have revealed anatomical structures in the cerebellum (Matsui et al., 2014) and hindbrain (Leyden et al., 2021; Schoonheim et al., 2010) which are involved in quick-phase eye movements. In comparison to the quick phase of OKR, spontaneous saccades in darkness can be internally driven by a ramping activity in hindbrain without any sensory input from the outside world (Ramirez & Aksay, 2021). However, the interval of these saccades can be regulated by the ambient luminance (Wolf et al., 2017). In mammals, the BDNs that anticipate quick phases also exhibit increased activity before and during spontaneous saccades (Kitama et al., 1992, 1995), suggesting a similar role of BDNs in planning both types of saccadic behavior.

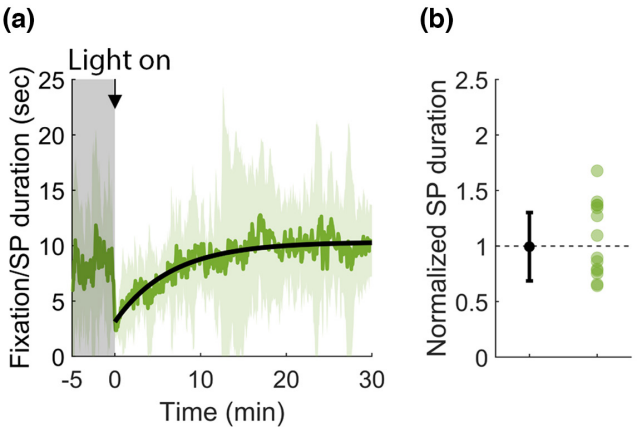

FIGURE 7 A comparison between fixation duration in darkness and the adapted SP duration after a prolonged stimulation. (a) The median ± median absolute deviation ($n = 14$) of right-eye fixation duration in the 5-min darkness and the following SP duration over 30-min OKR under 10-°/s stimulus. Pre-stimulus darkness is covered by gray-shaded area. The increased SP duration was fit by a first-order exponential curve as the black line. (b) SP duration in the last 5 s normalized by the pre-stimulus fixation duration in darkness. Green circles indicate the normalized SP durations of individual fish. Black circles ± error bars indicate median ± median absolute deviation of the population. Normalized SP duration is not significant different from 1 ($p = .426$, right eye; Wilcoxon signed rank test). Deg, degree; min, minute; OKR, optokinetic response; s, second; SP, slow phase.

In the current study, we observed a longer fixation duration of spontaneous saccades after a prolonged stimulus (Figure 5e). The concurrent and correlative rhythmic change of both saccadic behaviors suggests that either they share the underlying circuits for the saccadic initiation or they are initiated by different circuits and adapt to the same sensory input. Furthermore, the pre-stimulus fixation duration and the adapted SP durations under various stimulus conditions are statistically indistinguishable. This may suggest a preferred range of beating intervals that is close to the pre-stimulus fixation duration. Although the interval can be regulated by the sensory input in a short run, the saccadic initiator could adapt to a sustained input and adjust the interval to the preferred range in response. In other words, the saccadic frequency is maintained within a range in a homeostatic manner. Alternatively, both behavioral phenomena could be attributed to peripheral fatigue that affects oculomotor nerves and extraocular muscles. However, peripheral fatigue should impact eye velocity, rather than the onset of saccadic eye movements that are initiated centrally.

4.4 | Delayed quick phase may be a general developmental issue across species

Congenital ocular motor apraxia (COMA) is a neurodevelopmental disorder with saccadic deficits including prolonged saccadic latency and reduced saccadic amplitude (Shawkat et al., 1995; Zee et al., 1977). One of the most prevalent symptoms is the delayed horizontal quick phase after slow-phase eye tracking of either optokinetic response or vestibular nystagmus, and the consequence is the temporarily tonic deviation of the eyes which has been termed "lockup" clinically (Harris et al., 1996; Shawkat et al., 1995; Zee et al., 1977). Even though, in some cases, abnormality in brain areas such as vermal cerebellum could explain the saccadic inability (Harris et al., 1998; Marr et al., 2005), in a large number of patients without an examinable pathological cause, the etiology remains mostly unclear (Marr et al., 2005; Salman & Ikeda, 2013; Shawkat et al., 1995). COMA patients often show several developmental delays including in cognitive, language, and motor functions (Marr et al., 2005; Salman & Ikeda, 2013). Furthermore, the ocular motor symptoms appear to improve with age (Godel et al., 1979; Narbona et al., 1980; Prasad & Nair, 1994). Interestingly, a previous study describing a similar tonic deviation of the eyes in 5-day-old larval zebrafish has documented the disappearance of such behavior in elder animals (35 days post fertilization) (Beck et al., 2004). The similarity of the tonic eye deviation manifested at an early developmental stage in both fish and humans makes zebrafish a potential novel model for studying this eye movement disorder. It is possible that the lockup symptom in patients mainly reflects the immaturity of the saccadic system due to a general developmental delay instead of a specific underlying malfunction in the brain. Although a prolonged stimulus is not necessary to induce the eye lodging in zebrafish larvae (Beck et al., 2004), based on our results, a fast and long stimulus does increase the chance of observing such behaviors. In general, either a developmental delay or an extreme optokinetic stimulus may induce the deficient saccadic eye movements in young animals. Furthermore, a mutation in *dscaml1* gene can further enhance the chance of the saccade deficiency within only a short stimulus period in zebrafish larva (Ma et al., 2020). The tonic eye deviation observed in either genotype of larval zebrafish phenocopies the lockup symptom seen in COMA patients. Owing to several advantages including its highly developed visual system, zebrafish has been widely applied to model human eye diseases (Chhetri et al., 2014; Maurer et al., 2011). Based on our quantitative analysis, further studies can be designed based on the paradigms established in the current study.

DECLARATION OF TRANSPARENCY

The authors, reviewers and editors affirm that in accordance to the policies set by the *Journal of Neuroscience Research*, this manuscript presents an accurate and transparent account of the study being reported and that all critical details describing the methods and results are present.

AUTHOR CONTRIBUTIONS

Conceptualization, T.-F.L. and M.Y.H.; *Formal Analysis*, T.-F.L.; *Investigation*, T.-F.L.; *Data Curation*, T.-F.L.; *Writing – Original Draft*, T.-F.L.; *Writing – Review & Editing*, T.-F.L. and M.Y.H.; *Visualization*, T.-F.L.; *Supervision*, M.Y.H.; *Project Administration*, T.-F.L. and M.Y.H.; *Funding Acquisition*, T.-F.L. and M.Y.H.

ACKNOWLEDGMENTS

The authors thank Jeannie Wurz and Silas E. Busch for proofreading and editing the manuscript; Drs Frank Stüber and Markus Lüdi for providing the resources and support for carrying out this study.

FUNDING INFORMATION

This research was funded by research grant for the Faculty of Medicine, UZH (M.Y.H.), the Dr. Dabbous Foundation (T.-F.L. and M.Y.H.), EMDO Stiftung (M.Y.H., Gesuch Nr. 942), the Betty and David Koetser Foundation for Brain Research (T.-F.L. and M.Y.H.), and an institutional grant from the Department of Anaesthesiology and Pain Medicine, Inselspital, Bern (MYH, Gesuch Nr. HEYF-1-22).

CONFLICT OF INTEREST STATEMENT

The authors declare no conflict of interests.

PEER REVIEW

The peer review history for this article is available at https://www.webofscience.com/api/gateway/wos/peer-review/10.1002/jnr.25220.

DATA AVAILABILITY STATEMENT

The datasets generated for this study can be found at Zenodo via https://doi.org/10.5281/zenodo.5529443.

REFERENCES

Anastasio, T. J. (1996). A random walk model of fast-phase timing during optokinetic nystagmus. *Journal of Biological Cybernetics*, *75*(1), 1–9.

Beck, J. C., Gilland, E., Tank, D. W., & Baker, R. (2004). Quantifying the ontogeny of optokinetic and vestibuloocular behaviors in zebrafish, medaka, and goldfish. *Journal of Neurophysiology*, *92*(6), 3546–3561. https://doi.org/10.1152/jn.00311.2004

Chen, C. C., Bockisch, C. J., Bertolini, G., Olasagasti, I., Neuhauss, S. C., Weber, K. P., Straumann, D., & Ying-Yu Huang, M. (2014). Velocity storage mechanism in zebrafish larvae. *Journal of Physiology*, *592*(1), 203–214. https://doi.org/10.1113/jphysiol.2013.258640

Chhetri, J., Jacobson, G., & Gueven, N. (2014). Zebrafish—On the move towards ophthalmological research. *Eye*, *28*(4), 367–380. https://doi.org/10.1038/eye.2014.19

Dickinson, P. S. (2006). Neuromodulation of central pattern generators in invertebrates and vertebrates. *Current Opinion in Neurobiology*, *16*(6), 604–614. https://doi.org/10.1016/j.conb.2006.10.007

Fukushima, K., Fukushima, J., Ohashi, T., & Kase, M. (1991). Possible downward burster-driving neurons related to the anterior semicircular canal in the region of the interstitial nucleus of Cajal in alert cats. *Neuroscience Research*, *12*(4), 536–544. https://doi.org/10.1016/s0168-0102(09)80006-0

Godel, V., Nemet, P., & Lazar, M. (1979). Congenital ocular motor apraxia—Familial occurrence. *Ophthalmologica*, *179*(2), 90–93. https://doi.org/10.1159/000308872

Haffter, P., Granato, M., Brand, M., Mullins, M. C., Hammerschmidt, M., Kane, D. A., Odenthal, J., van Eeden, F., Jiang, Y. J., Heisenberg, C. P., Kelsh, R. N., Furutani-Seiki, M., Vogelsang, E., Beuchle, D., Schach, U., Fabian, C., & Nüsslein-Volhard, C. (1996). The identification of genes with unique and essential functions in the development of the zebrafish, *Danio rerio*. *Development*, *123*, 1–36.

Harris, C. M., Hodgkins, P. R., Kriss, A., Chong, W. K., Thompson, D. A., Mezey, L. E., Shawkat, F. S., Taylor, D. S., & Wilson, J. (1998). Familial congenital saccade initiation failure and isolated cerebellar vermis hypoplasia. *Developmental Medicine and Child Neurology*, *40*(11), 775–779. https://doi.org/10.1111/j.1469-8749.1998.tb12347.x

Harris, C. M., Shawkat, F., Russell-Eggitt, I., Wilson, J., & Taylor, D. (1996). Intermittent horizontal saccade failure ('ocular motor apraxia') in children. *British Journal of Ophthalmology*, *80*(2), 151–158. https://doi.org/10.1136/bjo.80.2.151

Huang, Y. Y., & Neuhauss, S. C. (2008). The optokinetic response in zebrafish and its applications. *Frontiers in Bioscience*, *13*, 1899–1916.

Huang, Y. Y., Rinner, O., Hedinger, P., Liu, S. C., & Neuhauss, S. C. F. (2006). Oculomotor instabilities in zebrafish mutant belladonna: A behavioral model for congenital nystagmus caused by axonal misrouting. *Journal of Neuroscience*, *26*(39), 9873–9880. https://doi.org/10.1523/jneurosci.2886-06.2006

Kitama, T., Ohki, Y., Shimazu, H., Tanaka, M., & Yoshida, K. (1995). Site of interaction between saccade signals and vestibular signals induced by head rotation in the alert cat: Functional properties and afferent organization of burster-driving neurons. *Journal of Neurophysiology*, *74*(1), 273–287. https://doi.org/10.1152/jn.1995.74.1.273

Kitama, T., Shimazu, H., Tanaka, M., & Yoshida, K. (1992). Vestibular and visual interaction in generation of rapid eye movements. *Annals of the New York Academy of Sciences*, *656*, 396–407. https://doi.org/10.1111/j.1749-6632.1992.tb25224.x

Leyden, C., Brysch, C., & Arrenberg, A. B. (2021). A distributed saccade-associated network encodes high velocity conjugate and monocular eye movements in the zebrafish hindbrain. *Scientific Reports*, *11*(1), 12644. https://doi.org/10.1038/s41598-021-90315-2

Lin, T. F., Mohammadi, M., Fathalla, A. M., Pul, D., Lüthi, D., Romano, F., Straumann, D., Cullen, K. E., Chacron, M. J., & Huang, M. Y. (2019). Negative optokinetic afternystagmus in larval zebrafish demonstrates set-point adaptation. *Scientific Reports*, *9*(1), 19039. https://doi.org/10.1038/s41598-019-55457-4

Ma, M., Ramirez, A. D., Wang, T., Roberts, R. L., Harmon, K. E., Schoppik, D., Sharma, A., Kuang, C., Goei, S. L., Gagnon, J. A., Zimmerman, S., Tsai, S. Q., Reyon, D., Joung, J. K., Aksay, E. R. F., Schier, A. F., & Pan, Y. A. (2020). Zebrafish dscaml1 deficiency impairs retinal patterning and oculomotor function. *Journal of Neuroscience*, *40*(1), 143–158. https://doi.org/10.1523/JNEUROSCI.1783-19.2019

Marr, J. E., Green, S. H., & Willshaw, H. E. (2005). Neurodevelopmental implications of ocular motor apraxia. *Developmental Medicine and Child Neurology*, *47*(12), 815–819. https://doi.org/10.1017/S0012162205001726

Matsui, H., Namikawa, K., Babaryka, A., & Koster, R. W. (2014). Functional regionalization of the teleost cerebellum analyzed in vivo. *Proceedings of the National Academy of Sciences of the United States of America*, *111*(32), 11846–11851. https://doi.org/10.1073/pnas.1403105111

Maurer, C. M., Huang, Y. Y., & Neuhauss, S. C. (2011). Application of zebrafish oculomotor behavior to model human disorders. *Reviews in the Neurosciences*, *22*(1), 5–16. https://doi.org/10.1515/RNS.2011.003

Miri, A., Bhasin, B. J., Aksay, E. R. F., Tank, D. W., & Goldman, M. S. (2022). Oculomotor plant and neural dynamics suggest gaze control requires integration on distributed timescales. *Journal of Physiology*, *600*(16), 3837–3863. https://doi.org/10.1113/JP282496

Mullins, M. C., Hammerschmidt, M., Haffter, P., & Nusslein-Volhard, C. (1994). Large-scale mutagenesis in the zebrafish: in search of genes controlling development in a vertebrate. *Current Biology*, *4*(3), 189–202.

Nakao, S., Sasaki, S., Schor, R. H., & Shimazu, H. (1982). Functional organization of premotor neurons in the cat medial vestibular nucleus related to slow and fast phases of nystagmus. *Experimental Brain Research*, *45*(3), 371–385. https://doi.org/10.1007/BF01208597

Narbona, J., Crisci, C. D., & Villa, I. (1980). Familial congenital ocular motor apraxia and immune deficiency. *Archives of Neurology*, *37*(5), 325. https://doi.org/10.1001/archneur.1980.00500540103026

Noorani, I., & Carpenter, R. H. (2016). The LATER model of reaction time and decision. *Neuroscience and Biobehavioral Reviews*, *64*, 229–251. https://doi.org/10.1016/j.neubiorev.2016.02.018

Ohki, Y., Shimazu, H., & Suzuki, I. (1988). Excitatory input to burst neurons from the labyrinth and its mediating pathway in the cat: Location and functional characteristics of burster-driving neurons. *Experimental Brain Research*, *72*(3), 457–472.

Otis, T. S. (2016). Simple spikes and complex spikes. In D. L. Gruol, N. Koibuchi, M. Manto, M. Molinari, J. D. Schmahmann, & Y. Shen (Eds.), *Essentials of cerebellum and cerebellar disorders* (pp. 299–303). Springer International Publishing.

Page-McCaw, P. S., Chung, S. C., Muto, A., Roeser, T., Staub, W., Finger-Baier, K. C., Korenbrot, J. I., & Baier, H. (2004). Retinal network adaptation to bright light requires tyrosinase. *Nature Neuroscience*, *7*(12), 1329–1336. https://doi.org/10.1038/nn1344

Pearson, K. G. (2000). Neural adaptation in the generation of rhythmic behavior. *Annual Review of Physiology*, *62*, 723–753. https://doi.org/10.1146/annurev.physiol.62.1.723

Pérez-Schuster, V., Kulkarni, A., Nouvian, M., Romano, S. A., Lygdas, K., Jouary, A., Dipoppa, M., Pietri, T., Haudrechy, M., Candat, V., Boulanger-Weill, J., Hakim, V., & Sumbre, G. (2016). Sustained rhythmic brain activity underlies visual motion perception in zebrafish. *Cell Reports*, *17*(11), 3089. https://doi.org/10.1016/j.celrep.2016.12.007

Portugues, R., Haesemeyer, M., Blum, M. L., & Engert, F. (2015). Whole-field visual motion drives swimming in larval zebrafish via a stochastic process. *The Journal of Experimental Biology*, *218*(Pt 9), 1433–1443. https://doi.org/10.1242/jeb.118299

Prasad, P., & Nair, S. (1994). Congenital ocular motor apraxia: sporadic and familial support for natural resolution. *Journal of Neuro-ophthalmology*, *14*(2), 102–104.

Qian, H., Zhu, Y., Ramsey, D. J., Chappell, R. L., Dowling, J. E., & Ripps, H. (2005). Directional asymmetries in the optokinetic response of larval zebrafish (*Danio rerio*). *Zebrafish*, *2*(3), 189–196. https://doi.org/10.1089/zeb.2005.2.189

Raman, I. M., & Bean, B. P. (1999). Ionic currents underlying spontaneous action potentials in isolated cerebellar Purkinje neurons. *Journal of Neuroscience*, *19*(5), 1663–1674.

Ramirez, A. D., & Aksay, E. R. F. (2021). Ramp-to-threshold dynamics in a hindbrain population controls the timing of spontaneous saccades. *Nature Communications*, *12*(1), 4145. https://doi.org/10.1038/s41467-021-24336-w

Salman, M. S., & Ikeda, K. M. (2013). The syndrome of infantile-onset saccade initiation delay. *Canadian Journal of Neurological Sciences*, *40*(2), 235–240. https://doi.org/10.1017/s0317167100013792

Schoonheim, P. J., Arrenberg, A. B., Del Bene, F., & Baier, H. (2010). Optogenetic localization and genetic perturbation of saccade-generating neurons in zebrafish. *Journal of Neuroscience*, *30*(20), 7111–7120. https://doi.org/10.1523/JNEUROSCI.5193-09.2010

Shawkat, F. S., Kingsley, D., Kendall, B., Russell-Eggitt, I., Taylor, D. S., & Harris, C. M. (1995). Neuroradiological and eye movement correlates in children with intermittent saccade failure: "ocular motor apraxia". *Neuropediatrics*, *26*(6), 298–305. https://doi.org/10.1055/s-2007-979778

Spence, R., Fatema, M., Reichard, M., Huq, K., Wahab, M., Ahmed, Z., & Smith, C. (2006). The distribution and habitat preferences of the zebrafish in Bangladesh. *Journal of Fish Biology*, *69*(5), 1435–1448.

Trillenberg, P., Zee, D. S., & Shelhamer, M. (2002). On the distribution of fast-phase intervals in optokinetic and vestibular nystagmus. *Biological Cybernetics*, *87*(1), 68–78. https://doi.org/10.1007/s00422-002-0324-3

Waddington, J., & Harris, C. M. (2013). The distribution of quick phase interval durations in human optokinetic nystagmus. *Experimental Brain Research*, *224*(2), 179–187. https://doi.org/10.1007/s00221-012-3297-z

Waddington, J., & Harris, C. M. (2015). Human optokinetic nystagmus and spatial frequency. *Journal of Vision*, *15*(13), 7. https://doi.org/10.1167/15.13.7

Wolf, S., Dubreuil, A. M., Bertoni, T., Böhm, U. L., Bormuth, V., Candelier, R., Karpenko, S., Hildebrand, D. G. C., Bianco, I. H., Monasson, R., & Debrégeas, G. (2017). Sensorimotor computation underlying phototaxis in zebrafish. *Nature Communications*, *8*(1), 651. https://doi.org/10.1038/s41467-017-00310-3

Wu, Y., Dal Maschio, M., Kubo, F., & Baier, H. (2020). An optical illusion pinpoints an essential circuit node for global motion processing. *Neuron*, *108*, 722–734.e5. https://doi.org/10.1016/j.neuron.2020.08.027

Zee, D. S., Yee, R. D., & Singer, H. S. (1977). Congenital ocular motor apraxia. *Brain*, *100*(3), 581–599. https://doi.org/10.1093/brain/100.3.581

SUPPORTING INFORMATION

Additional supporting information can be found online in the Supporting Information section at the end of this article.

Data S1

FIGURE S1 10 min of stimulation leads to OKR adaptation. Left-eye (a–c) SP duration, (d–f) SP velocity, and (g–i) SP amplitude under different stimulus velocities. Median of (a) SP durations, (d) SP velocities and (g) SP amplitudes among fish during the 10-min recording under 10, 20, 40, 60 and 80-°/s stimuli ($n = 23$, 19, 16, 15 and 17, respectively). (b), (e) and (h) show the magnifications of (a), (d) and (g), respectively, to demonstrate the initial 30 s of recordings. (c), (f) and (i) plot the statistical results of SP durations, SP velocities and SP amplitudes, respectively. P stands for peak SP velocities during the beginning of recordings. Average values during the first 5 s (early, E) and the last 5 s (late, L, or steady state, S) were calculated. Grey and colored circles indicate values of individual fish. Black circles ± error bars indicate the median ± median absolute deviation of populations. The population medians are linked by dotted line or solid line across stimulus conditions. Asterisks denote the significant difference levels ($^{*}p < .05$; $^{**}p < .01$; $^{***}p < .001$; Wilcoxon signed rank test). Deg, degree; min, minute; OKR, optokinetic response; s, second; SP, slow phase.

FIGURE S2 10 min of stimulation leads to adaptation of SP gain. (a) Median of SP gains among fish during the 10-min recording under 10, 20, 40, 60 and 80-°/s stimuli ($n = 23$, 19, 16, 15 and 17, respectively). (b) Shows the magnifications of (a) to demonstrate the initial 30 s of recordings. Deg, degree; min, minute; s, second; SP, slow phase.

FIGURE S3 SP time constants, phase-I and phase-II durations extend over 10 min of optokinetic stimulation. Left-eye (a–c) SP time constant, (d–f) phase-I duration and (g–i) phase-II duration under different stimulus velocities. Median of (a) SP time constants, (d) phase-I durations and (g) phase-II durations among fish during the 10-min recording under 10, 20, 40, 60 and 80-°/s stimuli ($n = 23$, 19, 16, 15 and 17, respectively). (b), (e) and (h) show the magnifications of (a), (d) and (g), respectively, to demonstrate the initial 30 s of recordings. (c), (f) and (i) plot the statistical results of SP

time constants, phase-I and phase-II durations, respectively, during the first 5-s (early, E) and the last 5-s (late, L). Grey and colored circles indicate values of individual fish. Black circles ± error bars indicate the median ± median absolute deviation of populations. The population medians are linked by dotted line or solid line across stimulus conditions. Asterisks denote the significant difference levels (*$p < .05$; **$p < .01$; ***$p < .001$; Wilcoxon signed rank test). Deg, degree; min, minute; s, second.

FIGURE S4 SP time constant is a good predictor of phase-I duration but not phase-II duration or SP duration. (a) Phase-I, (c) phase-II, and (d) SP durations plotted against time constants for slow phases of the left eye, respectively. (e, g, and h) The same plots for slow phases for the right eye. (b) and (f) show the magnifications of (a) and (e), respectively. Data were collected from 23, 19, 16, 15 and 17 fish under 10 min of 10, 20, 40, 60 and 80-°/s stimuli resulting in 2476, 1867, 1543, 1215, and 1267 right-eye slow phases and 2461, 1889, 1561, 1234, and 1296 left-eye slow phases, respectively. *p*, *p*-value of Pearson's correlation; *R*, Pearson's correlation coefficient.

FIGURE S5 Eye beating fields under different stimulus velocities. (a–e) Fields of eye movements during the 10-min recording, and the corresponding magnifications (f–j) of the first 30 s under 10, 20, 40, 60 and 80-°/s stimuli ($n = 23$, 19, 16, 15 and 17, respectively). Positive values represent movements to the left (counterclockwise), and negative values represent movements to the right (clockwise). Deg, degree; L, left direction; min, minute; R, right direction; s, second.

FIGURE S6 The extended drifting duration after SP-duration adaptation in the left eye. (a) The comparison of the SP durations between the first and last 5-min windows of the stimulation. (b) The comparison of drifting durations in darkness before and after the stimulation. Grey circles indicate average SP or drifting durations within each 5-min window of individual fish. Black circles ± error bars indicate median ± median absolute deviation of the population ($n = 29$). Asterisks denote the significant difference (***Wilcoxon signed rank test, $p < .001$). Data are collected from the left eye. Deg, degree; min, minute; s, second; SP, slow phase.

FIGURE S7 A comparison between the drifting duration in darkness and SP duration in different time periods. (a) A visual stimulation protocol showing 5-min darkness followed by 10 min of optokinetic stimulation with the stimulus velocities in 10, 20, 40, 60 and 80°/s ($n = 23$, 19, 16, 15 and 17, respectively). (b) and (c) SP durations in the first 5 s (early) and the last 5 s (late) of OKR, respectively, normalized by the pre-stimulus drifting duration (dark). Colored circles indicate the normalized SP duration of individual fish. Black circles ± error bars indicate median ± median absolute deviation of populations. Asterisks denote the significantly different than 1 (***Wilcoxon signed rank test, $p < .001$). Data are collected from the left eye. Deg, degree; min, minute; OKR, optokinetic response; s, second; SP, slow phase.

FIGURE S8 A comparison between fixation duration in darkness and the adapted SP duration after a prolonged stimulation. (a) The median ± median absolute deviation ($n = 14$) of left-eye drifting duration in the 5-min darkness and the following SP duration over 30-min OKR under 10-°/s stimulus. Pre-stimulus darkness is covered by grey shaded area. The increased SP duration was fit by a first order exponential curve as the black line. (b) SP duration in the last 5 s normalized by the pre-stimulus drifting duration in darkness. Green circles indicate the normalized SP durations of individual fish. Black circles ± error bars indicate median ± median absolute deviation of the population. Normalized SP duration is not significantly different from 1 ($p = .241$; Wilcoxon signed rank test). Deg, degree; min, minute; OKR, optokinetic response; s, second; SP, slow phase.

TABLE S1 *p*-values of multiple comparison tests using Dunn & Sidák's approach follow Kruskal-Wallis test ($p < .001$, left eye; $p < .001$, right eye) for the first 5-s SP durations among different stimulus velocity conditions (grey circles in Figure 3c and Figure S1c). Shaded areas in the table represent the *p*-values from the right eye, while the unshaded areas in the table represent *p*-values from the left eye. *$p < .05$; **$p < .01$; ***$p < .001$. Deg, degree; s, second; SP, slow phase.

TABLE S2 *p*-values of multiple comparison tests using Dunn & Sidák's approach follow Kruskal-Wallis test ($p = .368$, left eye; $p = .149$, right eye) for the last 5-s SP durations among different stimulus velocity conditions (colored circles in Figure 3c and Figure S1c). Shaded areas in the table represent the *p*-values from the right eye, while the unshaded areas in the table represent *p*-values from the left eye. Deg, degree; s, second; SP, slow phase.

TABLE S3 *p*-values of multiple comparison tests using Dunn & Sidák's approach follow Kruskal-Wallis test ($p < .001$, left eye; $p < .001$, right eye) for the first 5-s SP velocities among different stimulus velocity conditions (grey circles in Figure 3f and Figure S1f). Shaded areas in the table represent the *p*-values from the right eye, while the unshaded areas in the table represent *p*-values from the left eye. *$p < .05$; **$p < .01$; ***$p < .001$. Deg, degree; s, second; SP, slow phase.

TABLE S4 *p*-values of multiple comparison tests using Dunn & Sidák's approach follow Kruskal-Wallis test ($p < .001$, left eye; $p < .001$, right eye) for the last 5-s SP velocities among different stimulus velocity conditions (colored circles in Figure 3f and Figure S1f). Shaded areas in the table represent the *p*-values from the right eye, while the unshaded areas in the table represent *p*-values from the left eye. *$p < .05$; **$p < .01$; ***$p < .001$. Deg, degree; s, second; SP, slow phase.

TABLE S5 *p*-values of Wilcoxon signed rank test for the SP amplitudes between the first 5 s (grey circles in Figure 3i and Figure S1i) and the last 5 s (colored circles in Figure 3i and Figure S1i). *$p < .05$; **$p < .01$; ***$p < .001$. Deg, degree; s, second.

TABLE S6 *p*-values of multiple comparison tests using Dunn & Sidák's approach follow Kruskal-Wallis test ($p = .512$, left eye; $p = .704$, right eye) for the first 5-s SP amplitudes among different stimulus velocity conditions (grey circles in Figure 3i and Figure S1i). Shaded areas in the table represent the *p*-values from the right eye, while the unshaded areas in the table represent *p*-values from the left eye. Deg, degree; s, second; SP, slow phase.

TABLE S7 *p*-values of multiple comparison tests using Dunn & Sidák's approach follow Kruskal-Wallis test ($p = .578$, left eye; $p = .139$, right eye) for the last 5-s SP amplitudes among different stimulus velocity conditions (colored circles in Figure 3i and Figure S1i). Shaded areas in the table represent the *p*-values from the right eye, while the unshaded areas in the table represent *p*-values from the left eye.

Deg, degree; s, second; SP, slow phase.

TABLE S8 *p*-values of Wilcoxon signed rank test for the SP time constants between the first 5 s (grey circles in Figure 4f and Figure S3c) and the last 5 s (colored circles in Figure 4f and Figure S3c). $^{*}p < .05$; $^{**}p < .01$; $^{***}p < .001$. Deg, degree; s, second.

TABLE S9 *p*-values of multiple comparison tests using Dunn & Sidák's approach follow Kruskal-Wallis test ($p < .001$, left eye; $p < .001$, right eye) for the first 5-s SP time constants among different stimulus velocity conditions (grey circles in Figure 4f and Figure S3c). Shaded areas in the table represent the *p*-values from the right eye, while the unshaded areas in the table represent *p*-values from the left eye. $^{*}p < .05$; $^{**}p < .01$; $^{***}p < .001$. Deg, degree; s, second; SP, slow phase.

TABLE S10 *p*-values of multiple comparison tests using Dunn & Sidák's approach follow Kruskal-Wallis test ($p < .001$, left eye; $p < .001$, right eye) for the last 5-s SP time constants among different stimulus velocity conditions (colored circles in Figure 4f and Figure S3c). Shaded areas in the table represent the *p*-values from the right eye, while the unshaded areas in the table represent *p*-values from the left eye. $^{*}p < .05$; $^{**}p < .01$; $^{***}p < .001$. Deg, degree; s, second; SP, slow phase.

TABLE S11 *p*-values of multiple comparison tests using Dunn & Sidák's approach follow Kruskal-Wallis test ($p < .001$, left eye; $p < .001$, right eye) for the first 5-s phase-I durations among different stimulus velocity conditions (grey circles in Figure 4i and Figure S3f). Shaded areas in the table represent the *p*-values from the right eye, while the unshaded areas in the table represent *p*-values from the left eye. $^{*}p < .05$; $^{**}p < .01$; $^{***}p < .001$. Deg, degree; s, second; SP, slow phase.

TABLE S12 *p*-values of multiple comparison tests using Dunn & Sidák's approach follow Kruskal-Wallis test ($p < .001$, left eye; $p < .001$, right eye) for the last 5-s phase-I durations among different stimulus velocity conditions (colored circles in Figure 4i and Figure S3f). Shaded areas in the table represent the *p*-values from the right eye, while the unshaded areas in the table represent *p*-values from the left eye. $^{*}p < .05$; $^{**}p < .01$; $^{***}p < .001$. Deg, degree; s, second; SP, slow phase.

TABLE S13 *p*-values of multiple comparison tests using Dunn & Sidák's approach follow Kruskal-Wallis test ($p = .067$, left eye; $p = .020$, right eye) for the last 5-s phase-II durations among different stimulus velocity conditions (colored circles in Figure 4l and Figure S3i). Shaded areas in the table represent the *p*-values from the right eye, while the unshaded areas in the table represent *p*-values from the left eye. $^{*}p < .05$. Deg, degree; s, second; SP, slow phase.

TABLE S14 *p*-values of Wilcoxon signed rank test comparing the normalized SP durations with 1 in the first 5 s (early) and the last 5 s (late) of OKR (corresponding to the data shown in Figure 6 and Figure S7). $^{*}p < .05$; $^{**}p < .01$; $^{***}p < .001$. Deg, degree; s, second.

Transparent Science Questionnaire for Authors

How to cite this article: Lin, T.-F., & Huang, M.-Y. (2023). A quantitative approach to study the adaptation of rhythmic eye movements and the resulting tonic eye deviation in larval zebrafish. *Journal of Neuroscience Research*, *101*, 1504–1518. https://doi.org/10.1002/jnr.25220